Colloids and Surfaces B: Biointerfaces 145 (2016) 634–642

Contents lists available at ScienceDirect

Colloids and Surfaces B: Biointerfaces

journal homepage: www.elsevier.com/locate/colsurfb

Hybrid biomaterials based on calcium carbonate and polyaniline nanoparticles for application in photothermal therapy

Andrónico Neira-Carrillo[a,b,**], Edith Yslas[a,c,d], Yazmin Amar Marini[a,b], Patricio Vásquez-Quitral[a,b], Marianela Sánchez[a,b], Ana Riveros[b,d], Diego Yáñez[a,b], Pablo Cavallo[e], Marcelo J. Kogan[b,d], Diego Acevedo[e,*]

[a] Departamento de Ciencias Biológicas Animales, Fac. de Cs. Veterinarias y Pecuarias, Universidad de Chile, Av. Santa Rosa 11735, La Pintana, Santiago, 8820000, Chile
[b] Centro Avanzado de Enfermedades Crónicas (ACCDiS), Universidad de Chile, Sergio Livingstone 1007, Independencia, Santiago, 8380000, Chile
[c] Departamento Biología Molecular, Fac. CEF-Q y N, Universidad Nacional de Río Cuarto, CONICET, Ruta 36 km 601, Río Cuarto Cordoba, 5800, Argentina
[d] Departamento de Química Farmacológica y Toxicológica, Fac. Cs. Químicas y Farmacéuticas, Universidad de Chile. Sergio Livingstone 1007, Independencia, Santiago, 8380000, Chile
[e] Departamento de Química CONICET y Tecnología Química, Universidad Nacional de Río Cuarto. Ruta 36 km 601, Río Cuarto, Córdoba, 5800, Argentina

ARTICLE INFO

Article history:
Received 12 February 2016
Received in revised form 18 May 2016
Accepted 23 May 2016
Available online 24 May 2016

Keywords:
Biological applications of polymers
Biomineralization
Drug delivery systems
Nanocomposites
Nanoparticles

ABSTRACT

Inorganic materials contain remarkable properties for drug delivery, such as a large surface area and nanoporous structure. Among these materials, $CaCO_3$ microparticles (CMPs) exhibit a high encapsulation efficiency and solubility in acidic media. The extracellular pH of tumor neoplastic tissue is significantly lower than the extracellular pH of normal tissue facilitating the release of drug-encapsulating CMPs in this area. Conducting polyaniline (PANI) absorbs light energy and transforms it into localized heat to produce cell death. This work aimed to generate hybrid CMPs loaded with PANI for photothermal therapy (PTT). The hybrid nanomaterial was synthesized with $CaCO_3$ and carboxymethyl cellulose in a simple, reproducible manner. The CMP-PANI-Cys particles were developed for the first time and represent a novel type of hybrid biomaterial. Resultant nanoparticles were characterized utilizing scanning electron microscopy, dynamic light scattering, zeta potential, UV–vis, FTIR and Raman spectroscopy. *In vitro* HeLa cells in dark and irradiated conditions showed that CMP-PANI-Cys and PANI-Cys are nontoxic at the assayed concentrations. Hybrid biomaterials displayed high efficiency for potential PTT compared with PANI-Cys. In summary, hierarchical hybrid biomaterials composed of CMPs and PANI-Cys combined with near infrared irradiation represents a useful alternative in PTT.

1. Introduction

Calcium carbonate ($CaCO_3$) has been widely used in the development of hybrid organic-inorganic materials [1,2]. Primarily due to the properties $CaCO_3$ of compound: biocompatibility, large specific area, hierarchical structure, and mesoporosity [3–5]. This inorganic material can adsorb or encapsulate compounds [6] and deliver them in areas with an acidic pH, which is found in solid neoplastic tissues [7,8]. Bioinorganic materials possess key properties for drug delivery, such as a large surface area and nanoporous structure, [9] which permit loading of $CaCO_3$ microparticles (CMPs) with various drugs [10,11]. Alternatively, polyaniline (PANI) based organic-inorganic hybrid materials have been synthetized with interesting results, exhibiting improved or novel characteristics in comparison to those of the base PANI polymer [12,13].

In recent years photothermal therapy (PTT) has been extensively studied and compared to conventional chemo- and radiotherapy. This therapy is minimally invasive and can be actively delivered to specific biological targets using conductive particles [14,15]. Considering these advantages, PPT has emerged as a promising therapeutic modality for treating oncological disease. This therapy utilizes light in the near infrared (NIR) wavelength range of 700 nm–1200 nm and nanomaterials with good heat conduct-

* Corresponding author at: Departamento de Química-CONICET y Tecnología Química, Universidad Nacional de Río Cuarto. Ruta 36 Km 601, Río Cuarto, Córdoba, Argentina.
** Corresponding author at: Departamento de Ciencias Biológicas Animales, Fac. de Cs. Veterinarias y Pecuarias, Universidad de Chile, Av. Santa Rosa 11735, La Pintana, Santiago, 8820000, Chile.
E-mail addresses: aneira@uchile.cl (A. Neira-Carrillo), dacevedo@exa.unrc.edu.ar (D. Acevedo).

http://dx.doi.org/10.1016/j.colsurfb.2016.05.060
0927-7765/

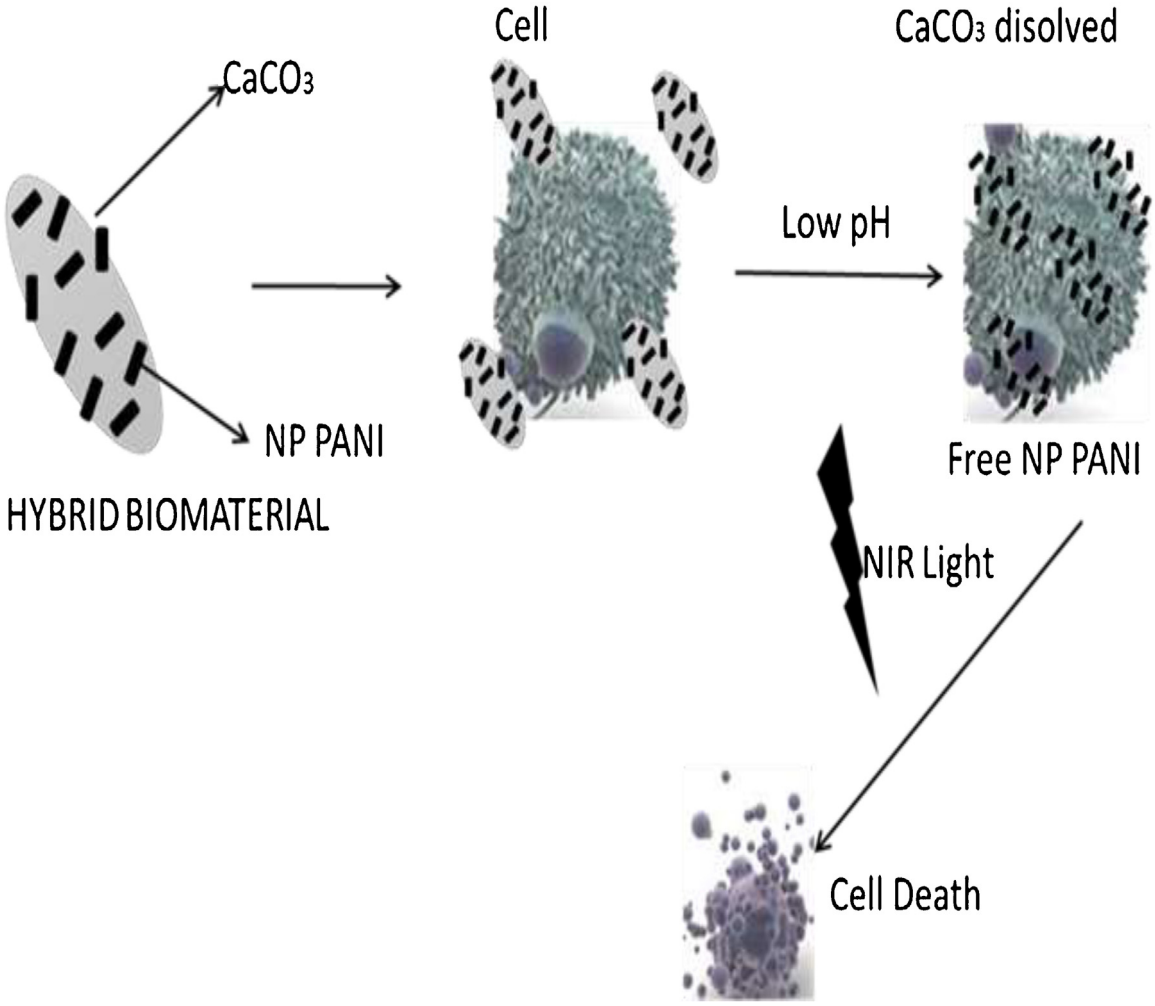

Scheme 1. Preparation of hybrid CMP-PANI-Cys microparticles and NIR laser irradiation of HeLa Cells.

ing properties. [16] Some nanomaterials absorb light in the NIR region, dissipating the radiation as heat [17,18]. In these nanomaterials absorbed photons are transformed into phonons in a process that involves rapid electron–phonon relaxation followed by phonon–phonon relaxation, resulting in increased system and, by conduction, surrounding temperature producing local heat [19]. NIR-induced PTT is particularly attractive because it is minimally absorbed by normal tissue and has relatively deep tissue penetration [20]. PANI particles absorb light energy then transform it into localized heat to produce controlled, local necrosis of neoplastic cells, which is termed photoablation [21].

This unique property of certain nanomaterials has been exploited to kill cancer cells. The hybrid materials used to synthesize advanced microparticles must contain numerous characteristics, such as a particular size and uniform shape, good solubility in an aqueous dispersion or solution, an excitation wavelength must be between 650 nm and 950 nm to avoid damaging the surrounding tissues, high photostability, and non-cytotoxic effects [22,23]. To locate these properties, different materials with conductive properties have been studied, such as graphene oxide [24], metallic nanoparticles [25], nanocomposites [26,27], and polymeric nanomaterials [14], among others [28]. Of the latter variety, PANI has generated great interest due to a low weight, mechanical flexibility, low cost, especially high electrical conductivity [29], low cytotoxicity [30], and biocompatibility [31], which are ideal for preparing hybrid microparticles utilized in PTT [21,22]. However, PANI exhibits low solubility in common solvents and it is not soluble in water medium, due to the balance hydrophilic/hydrophobic groups in the molecule [32]. Therefore, PANI modification with hydrophilic molecules such as L-cysteine can improve solubility in water-based media, maintaining both the conductivity and stability of the polymer [33]. Furthermore, research has demonstrated that the L-cysteine molecule improves biocompatibility to different materials. [34–37] Yslas et al. demonstrated that the modification of a PANI substrate with L-cysteine enhances cell attachment and growth in regard to unmodified PANI which is relevant to tissue engineering applications [34]. Liu et al. synthesized cysteine-coated CuS nanoparticles to operate as highly efficient PTT agents [35]. The Cys-CuS nanoparticles displayed high biocompatibility due to the biocompatible cysteine coating [35]. Moreover, Kesarkar et al. developed a facile method for impregnating a bi-functional linker L-cysteine onto gold nanoparticles [36]. The half-maximal cytotoxic concentration value of functionalized gold nanoparticles increased after conjugating with L-cysteine, improving biocompatibility [36]. The covalent immobilization of L-cysteine onto graphene oxide was recently demonstrated to improve uptake in zebrafish embryos, which showed no tissue defects, malformation, significant hatching delay, or death [37].

In view of the preceding information, this study aimed to generate biocompatible, hierarchical hybrid nanomaterials, composed of PANI modified with L-cysteine (PANI-Cys) and $CaCO_3$, which is able to incorporate the active photothermal nanomaterial (PANI) and deliver the loaded materials to an area with acidic pH near the cancer cells. (Scheme 1).

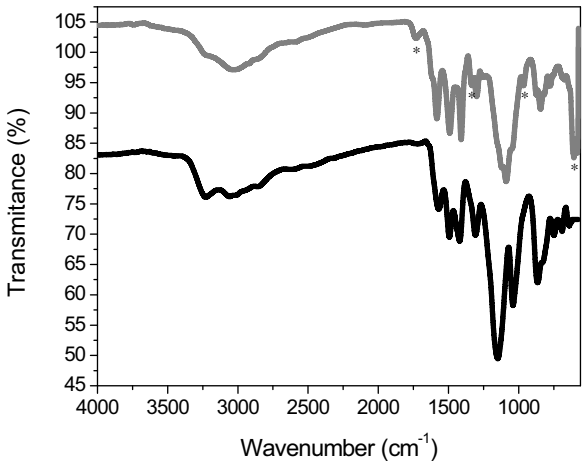

Fig. 1. FTIR spectra of PANI (gray line) and PANI-Cys (black line).

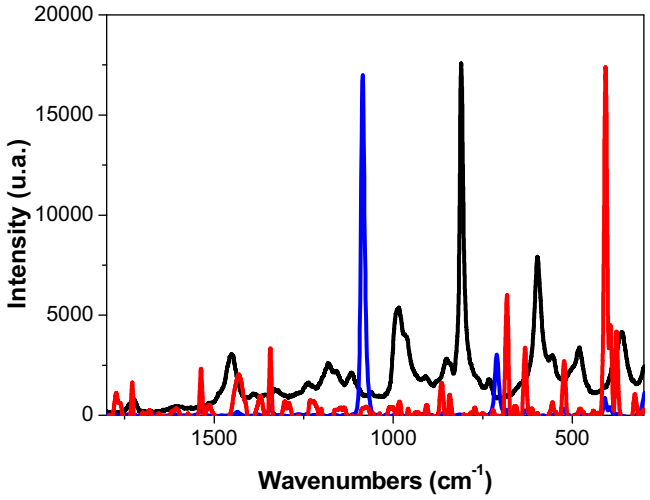

Fig. 2. Raman spectra of PANI-Cys (black line), CMPs (blue line) and hybrid biomaterial CMP-PANI-Cys (red line). (For interpretation of the references to colour in this figure legend, the reader is referred to the web version of this article.)

These hybrid materials were tested as NIR absorbent with potential biomedical applications in cancer PTT. Therefore, CMPs loaded with PANI-Cys were prepared in order to generate new biomaterials to improve cancer cell treatment. We report, for the first time, the preparation of a CMP-PANI-Cys hybrid biomaterial, by loading PANI nanoparticles modified with L-cysteine into CMPs. Moreover, this work showed that the application of these hybrid biomaterials improved PTT.

Our report demonstrated that hierarchical hybrid biomaterials composed of CMPs and PANI-Cys combined with irradiation are potentially useful new drug delivery systems due to the high efficiency for photothermal realease.

2. Results

2.1. Synthesis and characterization

FTIR spectroscopy was used to test the modification of the pristine polymer. The FTIR spectra of PANI (gray line) and PANI-Cys (black line) are shown in Fig. 1. The PANI spectrum displayed all characteristic polyaniline absorption bands: 1582 cm^{-1} (assigned to —C=N- stretching vibration of quinonimine rings) and 1492 cm^{-1} (C=C stretching vibration of aromatic rings) [38]. Also visible was the band at 1305 cm^{-1} corresponds to the stretching vibration of C—N, the band at 1147 cm^{-1}, which corresponded to the ring stretching N-Q-N, where Q represents the quinoid ring [38]. The broad conduction band in the range of 1800 cm^{-1} to 3500 cm^{-1} was assigned to the electronic transition in the free carriers of the polymer. [39,40] The FTIR spectrum of modified PANI-Cys showed additional absorption bands marked with an asterisk (*) in the graph at ~606 cm^{-1} that could be assigned to the C-S linkage of the cysteine group to the polymer. Additionally, new bands at 1731 cm^{-1} and 1333 cm^{-1} correspond to stretching of the C=O and C—O groups present in cysteine [34,41]. The infrared spectrum revealed that PANI-Cys exhibited new functional groups in comparison with unmodified PANI, confirming effective modification of the polymer.

FTIR of the hybrid material was also performed. However, the FTIR spectrum of the hybrid nanomaterial exhibited two strong absorption bands at 1400 cm^{-1} and 870 cm^{-1}, attributable to the presence of $CaCO_3$ and the high quantity of carbonate in the final CMP-PANI-Cys that avoid the visualization of PANI-Cys absorption bands that corresponds to the CMPs (Supporting information, S.I.-1). FTIR analysis of initial and hybrid materials is provided as supporting information (S.I.-2).

Raman spectroscopy was used to confirm the incorporation of PANI-Cys to the CMPs. Raman measurements for PANI-Cys (Fig. 2 dot line), CMP (Fig. 2 gray line), and hybrid materials CMP-PANI-Cys (Fig. 2 black line) were performed in an aqueous solution. The Raman spectrum of PANI-Cys showed a band at ~1700 cm^{-1} that could be assigned to the carboxylic cysteine group, a band with the maximum at 1470 cm^{-1} was attributable to the imine C=N vibration, and the semi benzenoid polaronic band at ~1350 cm^{-1} [42]. The band at 600 cm^{-1} could be assigned to C-S stretching of cysteine, and the imine deformation of quinoid units band was present at 800 cm^{-1} [43]. In the case of CMPs (Fig. 2 gray line), the Raman spectrum showed characteristic bands at 153, 278, 711 and 1085 cm^{-1} corresponding to the calcite polymorph of $CaCO_3$ [44]. The Raman spectrum of CMP-PANI-Cys (Fig. 2 black line) displayed a combination of initial PANI material and CMPs, which confirmed the formation of the hybrid biomaterial. These complementary results provided additional evidence demonstrating the incorporation of PANI-Cys by CMPs and successful formation of a hybrid biomaterial. Raman analysis of initial and hybrid materials is also provided as supporting information. (S.I.-3).

The morphology of the PANI-Cys nanoparticles was analyzed by scanning electron microscope (SEM) at a pH 2 and 7. The CMPs were solid, agglomerated spheres, with diameter ~30 nm (Fig. 3). The agglomeration of CMP could occur due to the direct electrostatic interaction between the carboxylate groups of the carboxymethyl cellulose (CMC) with the CaCO3, where the particles tend to agglomerate strongly. This process is dominated by the surface free energy during the aqueous interfacial method [45,46]. These agglomerates exhibited an elongated morphology, ranging from 1 μm to 500 nm in length and ~100 nm wide. No considerable differences were observed in the morphology at different pH values. The above mentioned materials were also analyzed by dynamic light scattering (DLS). The PANI-Cys at pH 2 was 553 nm with a polydispersity index (PdI) of 0.309 nm. The same material at pH 7 shows a size of 582 nm and PdI of 0.292. These values are larger than pristine PANI at pH 2 (481 nm, PDI 0.245) and pH 7 (382 nm, PDI 0.214). However, it is important to mention that DLS estimates the radius of the particles assuming a spherical shape, but miscalculations due to the asymmetric forms of the particles in the samples can not be discarded. This result could be explained by considering that the modification of the polymer backbone produced a steric effect that altered the morphology.

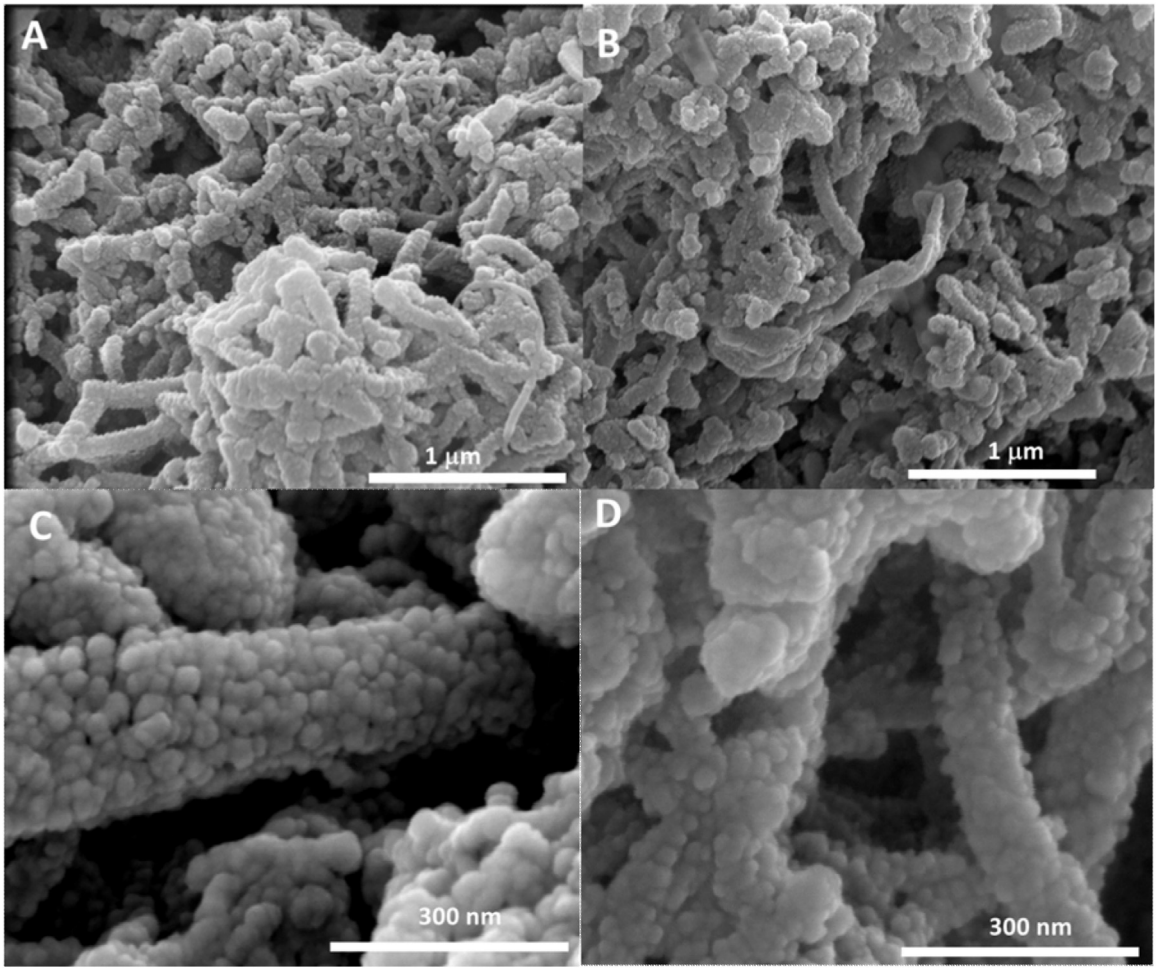

Fig. 3. SEM images of PANI-Cys obtained by evaporation of the polymer solution at pH 2 (A, C) and 7 (B, D) at different magnification.

Table 1
Sizes and zeta potential of CMPs and CMP-PANI-Cys.

	CMPs	CMP-PANI-Cys
Average diameter (nm)	1771 ± 81	780 ± 46
PdI	0.005	0.005
ζ (mV)	−31 ± 1	−35 ± 2

Values of zeta potential (ζ) for PANI at pH 2 and 7 were 9 ± 2 mV and −22 ± 2 mV respectively, and for PANI-Cys at pH 2 and 7 were 5 ± 5 and −24 ± 1 mV, respectively. These results could indicate that at a higher pH, deprotonation of the amino groups present in the polymer rendered a more negative ζ value.

The shape of CMPs was observed by SEM images (Fig. 4A). The formation of CMPs was also observed, with sizes ranging from 0.5 μm to 5 μm. The microparticles displayed a smooth surface with defined edges and a spherical to ovular shape. The morphology of the new hybrid biomaterial composed of CMP-PANI-Cys was analyzed by SEM (Fig. 4B). The hybrid biomaterial was ovular shape with an irregular surface due to the presence of the polymer and a particle size between 0.5 μm to 2 μm. Analysis of the SEM images let to the proposition that $CaCO_3$ microspheres with a mean diameter of 5 μm acted as a scaffold, providing numerous micro- or nanopores for the insertion of polymer nanoparticles.

The hybrid CMP-PANI-Cys was smaller than the CMPs, which was determined by DLS measurement (Table 1). This result concurred with the sizes observed by SEM. The decreased CMP-PANI-Cys size could be attributed to the electrostatic interaction between the amino groups (-NH_2) of PANI-Cys and the carboxylate group from $CaCO_3$. The more negative ζ value of CMP-PANI-Cys compared to CMPs was probably due to the incorporation and surface exposure of the PANI-Cys (Table 1).

Typical UV–vis spectrum of the PANI-Cys in DMSO is depicted in Fig. 5. Two characteristic absorption peaks at 340 nm and 602 nm appeared, corresponding to the $\pi \rightarrow \pi^*$ transition of the benzene rings and the exciton absorption of quinoid rings, respectively [47].

A standard calibration curve was established to obtain the concentration of hybrid material. The equation Abs = 0.0062 x C with R = 0.997281 was obtained, where C is the concentration of PANI-Cys in mg/mL. The standard calibration curve was used to determinate the incorporation efficiency (IE), the loading capacity (LC), and the performance (R). The UV–vis measurement of PANI-Cys was conducted by measuring the initial PANI-Cys concentration in solution and the concentration in the supernatant (unincorporated CMPs) before the formation of hybrid material. The incorporation parameters of PANI-Cys into the hybrid biomaterial such as IE, LC, and R were calculated by using Eqs. (1)–(3). The IE values (~81%) indicated a high percentage of PANI-Cys present in CMPs in regard to the total PANI-Cys, which is very favorable for production. The LC was ~0.7% indicating that the mass of modified materials was low in comparison to the mass of CMPs in the CMPs formulation. The R was ~28% because, of all the reagents used in the formulation, only certain molecules reacted to form particles (Ca^{2+} and $CO_3{}^{2-}$), and the rest were discarded.

$$IE = \frac{(\text{PANI} - \text{Cys} - \text{O}) - (\text{PANI} - \text{Cys} - \text{F})}{(\text{PANI} - \text{Cys} - \text{O})} \quad (1)$$

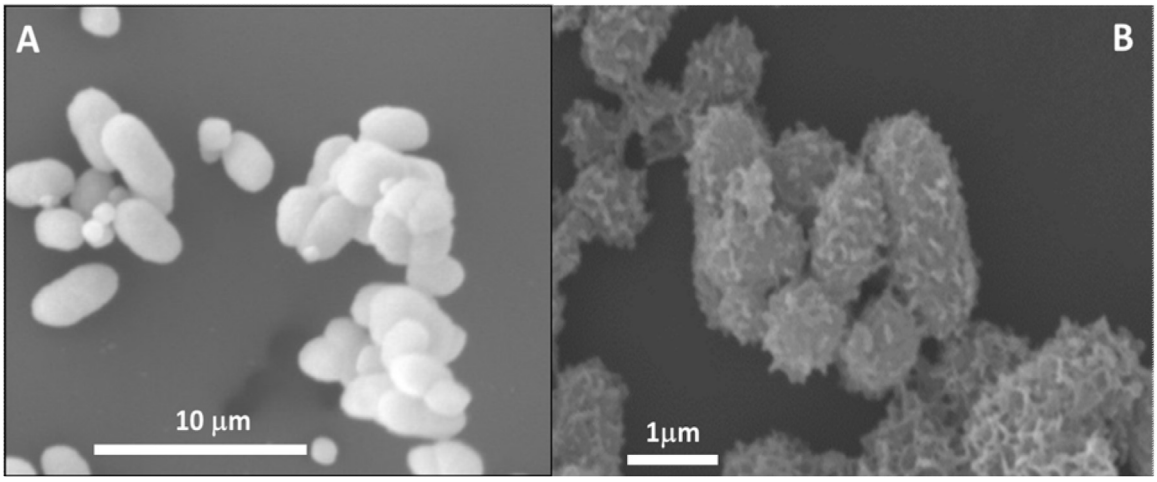

Fig. 4. SEM images of A) CMPs and B) CMP-PANI-Cys biomaterial.

$$LC = \frac{(PANI - Cys - O) - (PANI - Cys - F)}{MPw} x100 \quad (2)$$

$$R = \frac{MPw}{Mw + (PANI - Cys - O)} x100 \quad (3)$$

To evaluate the effect of pH variation of CMP-PANI-Cys solutions on the release of PANI-Cys nanoparticles, 6.25 mg/mL each of various hybrid formulations of CMP-PANI-Cys with pH values from pH 1.5 to pH 7.4 (adjusted with HCl) were incubated at 37 °C. The UV–vis spectra of PANI-Cys at 5 min, 30 min, 60 min, and 180 min (S.I.-4) and the percentage (%) of released PANI-Cys (S.I.-5) at 5 min from CMP-PANI-Cys hybrid particle in DMSO:H_2O (1:9) was evaluated by DLS and UV–vis. Considering a PANI-Cys incorporation of 81% into the CMPs-PANI-Cys hybrid formulations, the results indicated that in acidic media (pH 1.5) ~50% of released PANI-Cys particles were determined at 5 min. Longer times and pH values up to 3.0 had no statistical significance and determining a released PANI-Cys percentage higher than 8% was not possible. A complimentary control experiment was performed to evaluate the UV–vis absorbance influence of CMPs for PANI-Cys determination after the centrifugation of the CMP-PANI-Cys formulations (S.I.-5). Therefore, UV–vis of CMPs and PANI-Cys was carried out before and after centrifugation at 1740xg for 4 min with 0.1 mg/mL in DMSO:H_2O (1:9) (S.I.-5). An aliquot of CMP supernatant, instead of PANI-Cys, displayed an absorbance less than 0.00 (a.u.) at λ 310 nm, which demonstrated that the release of CMPs from CMP-PANI-Cys were unlikely to interfere with PANI-Cys determination.

The effect of CMP-PANI-Cys and the component PANI-Cys and CMPs on HeLa cells viability was investigated using the MTS assay. This assay showed that different concentrations of CMP-PANI-Cys, CMPs and PANI-Cys were nontoxic to cells treated for 24 h. Corresponding cell survival values for the different biomaterials are shown in Fig. 6. The CMPs and CMP-PANI-Cys, at concentrations lower than 2170 μg/mL and 2185 μg/mL, respectively, had no effect on cell viability. Furthermore, the concentration of CMP-PANI-Cys necessary to induce effects on cell viability in these trials was higher than the results obtained with other biomaterials reported in the literature [48,49].

2.2. Laser treatment of HeLa cells

Cells irradiated only with the NIR laser for 20 min and control cells displayed no change in the viability percentage. This result demonstrated that the NIR laser alone did not induce cell death at the assayed doses (Fig. 7). Alternatively, cells incubated with PANI-Cys and irradiated with NIR laser light for 20 min showed

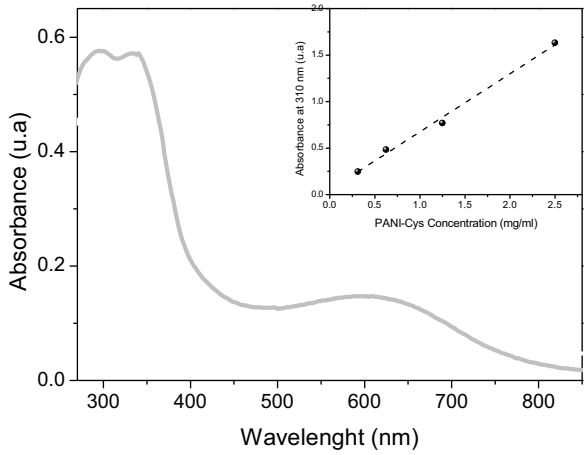

Fig. 5. UV–vis of PANI-Cys in DMSO and PANI-Cys absorbance versus concentration in DMSO (Insert).

49% cell viability. Cells incubated with the irradiated hybrid biomaterial CMP-PANI-Cys displayed significantly lower cell viability (38%). The data indicate that the hybrid biomaterial triggered more efficient PTT effect than PANI-Cys.

3. Discussion

In recent years, the synthesis of inorganic materials with controlled morphology and polymorphism has garnered the attention and interest of chemists due to the wide applicability of the materials. One of the most abundant biominerals, $CaCO_3$ has gained prominence in many fields and was found to be an ideal candidate for drug delivery because it has large porosity and surface area and can rapidly decompose under relatively mild conditions [50]. This biomaterial could be a potential carrier of various drugs [6,8,51–53]. Zhang et al. demonstrated that, though CMPs may induce oxidative damage to HeLa cells, porous, spherical $CaCO_3$ appeared to have good biocompatibility in comparison to other nanomaterials [54]. The results implied that CMPs could be utilized as relatively safe drug vehicles but that the effect of high dosages should not be ignored when attempting to maximize therapeutic activity by increasing the concentration [54]. Concurring with this observation, the MTS assay showed that PANI-Cys and CMP-PANI-Cys materials were nontoxic to the HeLa cell line. The CMP and CMP-PANI-Cys low effects on cell viability at concentra-

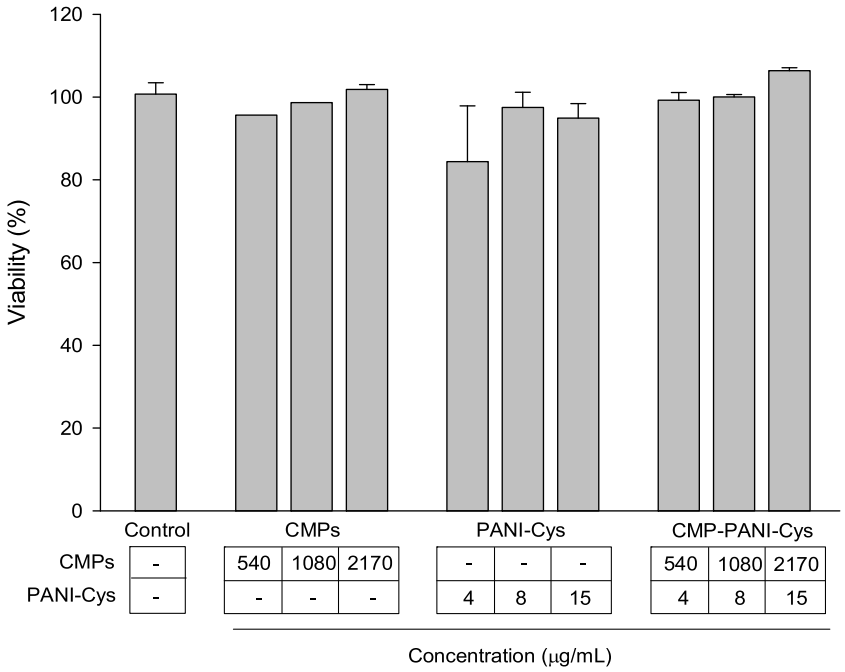

Fig. 6. Effects on cellular viability in HeLa cells against samples dark experiment. Control: untreated control cells, CMPs, PANI-Cys and CMP-PANI-Cys at different concentrations of each material (μg/mL). The table below the graphic shows the different concentrations of separated components (PANI-Cys and CMPs) and CMP-PANI-Cys. Values represent mean ± standard error of the mean of three separate experiments in triplicate.

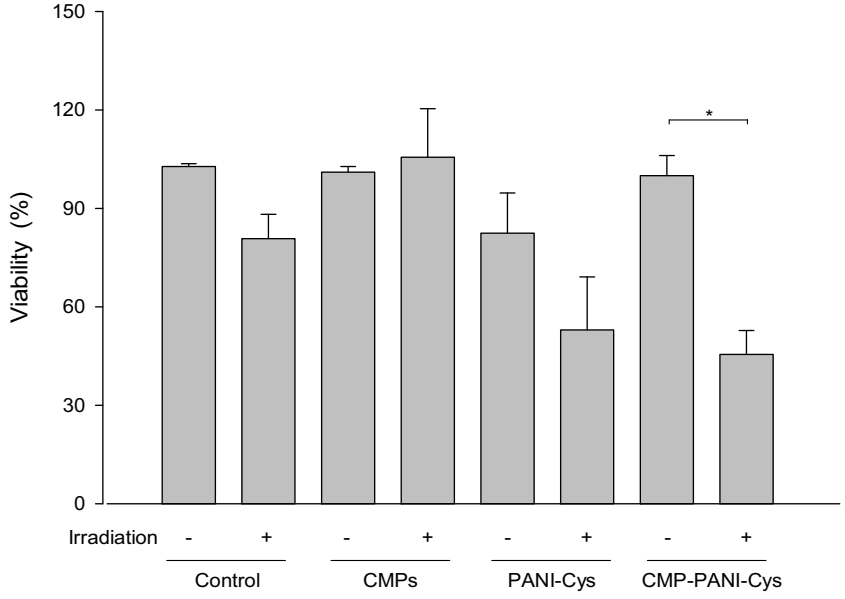

Fig. 7. Effects on cell viability post irradiation in HeLa cells. Control: untreated control cells. Control irradiated, CMPs (1080 μg/mL), PANI-Cys (8 μg/mL), and CMP-PANI-Cys (1088 μg/mL) in dark and irradiation conditions. The concentrations of PANI-Cys and CMPs were the same at those included in CMP-PANI-Cys. Values represent mean ± standard error of the mean of three separate experiments in triplicate. Statistical differences were assessed by ANOVA and Dunnís post test *$p < 0.05$.

tions lower than 2170 μg/mL and 2185 μg/mL, respectively, were demonstrated. Another important result was that the concentration values of CMP-PANI-Cys that induce toxic effects were very high compared to other nanomaterials [48,49].

Drug delivery systems are designed to promote and enhance the efficacy of controlled drug release by delivering therapeutic agents specifically and selectivity at the necessary sites without affecting the healthy neighboring cells or tissues. CMPs displayed promising potential in the development of anticancer drugs carriers. For example, porous CMPs are capable of simultaneously encapsulating and incorporating the protein co-precipitated with $CaCO_3$ [55]. We demonstrated that the CMP-PANI-Cys biomaterial was easily produced, with CMPs displaying a spherical to ovular shape that ranged from 0.5 μm to 5 μm in size. The $CaCO_3$ microspheres were utilized as a template due to the porosity of the surface, which provided numerous attachment sites for PANI-Cys. These results concurred with the data reported by Peng et al. on carboxymethyl cellulose (CMC), doped CMPs with a diameter of 5 μm, coated by chitosan and alginate multilayers [56]. These particles exhibited a strong Doxorubicin hydrochloride (DOX) loading ability, which was primarily attributed to the charge attraction between negatively charged CMC and positively charged DOX. This system has poten-

tial applications for *in vivo* drug delivery because the compound is only released under acidic conditions. Using similar concept, biogenic $CaCO_3$ has come to the attention of many researchers as a promising drug delivery system due to the safety, pH sensitivity, and the large volume of information available regarding medical use of $CaCO_3$. Other researchers have used CMPs for encapsulating Camptothecin, an effective anticancer agent, by diffusion and adsorption. Studies demonstrated that drug release was negligible under physiological conditions (pH = 7.4) but almost complete at a pH of 4–6, *i.e.* pH found in lysosomes and solid tumor tissue, respectively [9]. These findings suggest that porous, biogenic CMPs could be promising carriers for the safe and efficient delivery of anticancer drugs with low aqueous solubility. Cheng et al. encapsulated DNA/DOX in nano-sized $CaCO_3$ co-precipitates for co-delivery of genes and drugs [57]. The results indicated that simultaneous treatment with genes and drug could induce cell apoptosis and completely inhibit cell proliferation. Compared with the gene delivery system ($CaCO_3$/DNA NPs) or the free drug DOX, the co-delivery system exhibits enhanced cell inhibition rate. Abdullahi Kamba et al. developed and demonstrated a bio-based $CaCO_3$ nanocrystal carrier that could be loaded with an anticancer drug and would selectively deliver it to cancer cells with high specificity, achieving effective osteosarcoma cancer cell death without inducing specific toxicity [58]. The results indicated pH sensitivity of the controlled release characteristics of the drug. At a normal physiological pH of 7.4, ~80% of the drug was released within 1200 min but when exposed to a pH of 4.8 a similar amount was released in 50 min. This study showed that the DOX-loaded $CaCO_3$ nanocrystals have promising applications in the delivery of anticancer drugs. The IE values (81%) obtained in our materials indicate that a high percentage of PANI-Cys are presents in CMPs, which concurred with several studies that indicated the high compound loading capability of $CaCO_3$. Other researchers focused their studies on PTT materials for improvement of anticancer treatments [28]. Many materials have been examined, among PANI them, that offer the advantages of easy synthesis, high stability, and several possibilities for structural modification. In this context, the efficacy, toxicity, and effect on hepatic and kidney function of PANI nanoparticle- mediated PTT were assessed in a tumor-bearing mice model [21]. Ibarra *et al.,* demonstrated the high PTT efficacy of PANI nanoparticles followed by NIR light exposure. Considering the efficiency and biocompatibility of $CaCO_3$ and the effectiveness of PANI in PPT therapies, we synthetized and characterized a new biomaterial that presented those properties. Moreover, due to the solubility of carbonate in acidic media, which is typical of the neoplastic stroma or the tissue surrounding neoplastic growths, we proposed that the polymer will be undelivered near the cell cancer and increase the effectiveness of PPT.

The MTS results demonstrated that the viability percentage of cells incubated with the hybrid biomaterial CMP-PANI-Cys and then irradiated decreased to 38%, suggesting that the biomaterial triggered a better photothermal effect than PANI-Cys. In summary, we obtained an ovular CMP-PANI-Cys hybrid biomaterial with irregular surfaces through direct incorporation of PANI-Cys nanoparticles into porous $CaCO_3$ microspheres. This production strategy could be used to create a variety of complex, multifunctional biomaterials with a vast scope of applications, from biomedicine to nanotechnology and biomaterials science. We demonstrated that CMP-PANI-Cys was easy to synthetize and enhanced the potential cancer PTT.

4. Conclusions

Hybrid CMP-PANI-Cys materials composed of PANI nanoparticles functionalized with L-cysteine were synthesized and effectively incorporated into CMPs. The CMC was used to preserve the shape, composition, and long term stability of hybrid materials and to deliver the load near the cancer cell, which was released in the low pH areas that the cells induce. A simple way to synthesize hybrid microparticles was depicted. Raman and FTIR spectroscopies, as well as microscopic characterization, confirmed that PANI-Cys was incorporated into the nanopores of CMPs. SEM observation of CMPs showed defined edges, a smooth surface, and a spherical to ovular shape ranging from of 500 nm to 5 μm in size. Moreover, SEM analysis of the hybrid biomaterial indicated particles sizes between 500 nm and 2 μm, with defined edges, rough surfaces, and ovular shape. *In vitro* studies of the CMPs showed slight changes in cell survival at different concentrations and in dark and irradiated conditions. Hybrid CMP-PANI-Cys and PANI-Cys biomaterials did not induce changes in cell viability at the studied concentrations in dark conditions, but the combination of a laser in the NIR region and CMP-PANI-Cys markedly decreased cell viability. In summary, we concluded that the resultant hybrid biomaterial could be used a PTT agent for cancer ablation and the development concept used for PANI-based micro or nanobioparticles could serve as a platform for the next generation of *in vivo* cancer PTT agents.

5. Experimental

Reagents: Aniline (Sigma-Aldrich, St. Lous, MO, USA) was distilled twice. Ammonium peroxydisulfate (Sigma-Aldrich) was used without further purification. Hydrochloric acid (Cicarelli Laboratories, San Lorenzo, Argentina) was used as received. Calcium chloride dihydrate (Merck & Co., Kenilworth, New Jersey, USA) was used without any purification. Sodium carbonate monohydrate ≥ 99.5% and low viscosity carboxymethyl cellulose sodium salt were purchased from Sigma Aldrich. Dimethilsulfoxide (DMSO) 99.9% for analysis was from Winkler Ltda (Santiago, Chile). All aqueous solutions were prepared using milli-Q water. Other chemicals were analytical reagents and used as received.

Synthesis of PANI nanoparticles: To prepare the PANI nanoparticles, 7 mmol of aniline were mixed with 20 mL of bidistilled water and kept under a magnetic-bar stirrer for 30 min. Then, the mixture was cooled to 0 °C. An aqueous solution of ammonium peroxydisulfate (7 mmol) was dissolved in 80 mL of freshly distilled water and added to the aniline solution [59]. The reaction mixture was stirred for 1 h to complete the polymerization. The resultant PANI was collected on a filter paper, washed with distilled water, and dried under a vacuum for 1 day. The PANI was rinsed with 0.1 M NH_4OH solution and then collected and dried as described in the previous sentence to obtain emeraldine base, the deprotonated form of PANI. The polymer was functionalized by nucleophilic addition following the procedure described by Yslas *et al. [*34] The polymer was immersed into a stirred 1 M aqueous solution of L-cysteine for 24 h at room temperature, and then filtered, washed with deionized water, dried, and stored at room temperature.

Synthesis of CMPs: The CMPs were synthesized based on $CaCO_3$ and carboxymethyl cellulose (CMC) components by mixing 100 mL of aqueous 0.025 M $CaCl_2$ with 2 mL of CMC 5% w/v under a magnetic stirrer for 15 min (Solution A). Solution B was prepared by dissolving Na_2CO_3 in 100 mL of aqueous solution to obtain a 0.025 M solution, and rapidly added to Solution A under ultrasonication for 10 min using a Branson Digital Sonifier 450 (Branson Ultrasonic Corp., Danbury, CT, USA). CMPs were filtered with a 0.45 μm filter (Merck Millipore, Billerica, MA, USA) and washed with milli-Q water. Milli-Q water was obtained from a water purification system (Labostar^{TM} TWF, Evoqua Water Technologies LLC, Warrendale, PA, USA). The resultant CMPs were dried at room temperature.

Synthesis of a CMP-PANI-Cys Hybrids Materials: The CMP-PANI-Cys material was synthesized based on CMPs and the PANI-Cys polymer. The incorporation of PANI-Cys was performed in suspension. Briefly, 1 mL of a PANI-Cys stock solution was taken from a starting stock suspension. The concentrated stock solution was composed of 500 μL of PANI-Cys and 7.5 mL of PBS at pH 7.4, for a total of 1.8 mg of PANI-Cys in 1 mL of suspension. The suspension was then mixed with 100 mL of Solution B under magnetic stirrer until a homogenous suspension was obtained. This suspension (Solution B + PANI-Cys) was added to 100 mL of Solution A under ultrasonication at 80 W for 10 min. CMP-PANI-Cys materials were filtered with 0.45 μm filter and washed with milli-Q water.

Fourier Transform Infrared (FTIR) Spectroscopy: FTIR spectra of all materials were obtained with an ATR/FTIR interspec 200-X spectrometer (Interspectrum OU, Toravere, Estonia). The spectroscopic measurements of samples were performed directly using the PIKE MIRacle^{TM} accessory in a Ge single reflection crystal plate. A flat pressure tip was used for all FTIR spectra. The resolution was set to 4 cm^{-1} and 20 scans were averaged. The wavenumber range of the spectra was 600 cm^{-1} to 4000 cm^{-1}.

Ultraviolet-Visible Spectroscopy (UV–vis): UV–vis spectra were measured in a Rayleigh UV-2601 (Beijing Beifen-Ruili Analytical Instrument Co., Beijing, China). All the solutions were measured using a quartz cell with a 1 cm optical path. The concentration of PANI-Cys incorporated into the CMPs was determined by UV–vis spectroscopy (UV–vis 2601) using a standard calibration curve of the hybrid materials dissolved in DMSO. All samples were measured by transmission in a quartz cell with a 1 cm optical path. A standard calibration curve of PANI-Cys in DMSO was performed using UV–vis spectrophotometer at 340 nm. Three experiments were conducted to synthetize CMP-PANI-Cys by adding 50 mg of PANI-Cys to 2 mL of DMSO and were used to determine the incorporation efficiency (IE), loading capacity (LC) and production yield (R). Then, the solution was vortexed, centrifuged at 1740 xg for 4 min and the supernatant was removed.

Raman Spectroscopy: Raman spectra was obtained with a LabRam spectrometer (Horiba Scientific, Irvine, CA, USA). This system has a highly sensitive detection method and it uses a single spectrograph equipped with a notch filter in order to filter the Rayleigh scattering and holographic gratings (1800 and 600 grooves mm^{-1}). The slit and pinhole employed were 300 and 500 μm, respectively. The excitation line was provided by a 17 mW He-Ne laser at 632.8 nm and the laser power delivered at the sample ranged from 0.12 to 1.2 mW (laser power was kept under minimum values in order to prevent sample degradation). The laser beam was focused through a 50-x long working objective (0.5 NA). The diameter of the laser beam spot on the sample surface was 2 μm. The sample viewing system consisted of a color television camera attached to the microscope. The spectrometer resolution was 3 cm^{-1} and the detector was a Peltier-cooled charge-coupled device (1064 × 256 pixels).

Scanning Electron Microscopy: SEM images of the samples were observed in a LEO 1420VP SEM equipped with a dispositive for surface element microanalysis and a linear profile at 15 kV and in a Tesla 343 A SEM instruments. To obtain the SEM images, PANI-Cys were dispersed in buffer solution with a pH of 2 and 7 and dried before observation. CMPs and CMP-PANI-Cys were also observed by SEM.

Dynamic Light Scattering (DLS) and Z Potential: Particle size and zeta potential (ζ) of the PANI, PANI-Cys, CMPs and CMP-PANI-Cys were estimated using a ZetaPlus analyzer and a 90 Plus/BI-MAS (Brookhaven Instruments Corp., Holtsville, NY, USA). The overall concentration of PANI-Cys was represented by PANI-Cys-O, and PANI-Cys-F corresponded to the quantity of polymer that remained in the solution post-encapsulation. MPw is the weight of the microparticles and Mw is the overall weight of the materials employed in hibrid synthesis. DLS analysis was performed at 25 °C by using a Malvern Zetasizer Nano ZS operating at a light source wavelength of 532 nm with a fixed scattering angle of 90°. Measurements were performed by introducing 1 mL of the colloidal sample in a cell with an optical path of 1 cm. To determine the size distribution of the samples, the results were analyzed from the intensity distribution values using the cumulants method [60].

Cell Viability Assay: To determine the effect of the PANI-Cys, CMPs and CMP-PANI-Cys on cell viability, an MTS assay was performed. A linear relationship between the viable cell number and absorbance can be establish by the MTS test. The HeLa cells were seeded on 96-well plates at 2500 cells per well in low glucose Dulbecco's modified Eagle's medium (DMEM), containing 5% inactivated fetal calf serum (FCS), 2 mM glutamine, 50 U/mL penicillin, and 0.05 g/mL streptomycin. The cells were then treated with increasing concentrations of CMP-PANI-Cys, PANI-Cys, CMPs and CMP-PANI-Cys. After 24 h of incubation, cell viability was measured in triplicate in three independent experiments using the MTS assay according to manufacturer's protocol.

Laser Treatment of HeLa Cells: The HeLa cells were seeded on 96-well plates at 2500 cells per well in Dulbecco's modified Eagle's medium. Then, cells were incubated with PANI-Cys, CMP and new hybrid CMP-PANI-Cys for 24 h. The cancer cell samples were irradiated using NIR irradiation with a light fluence of 500 mW/cm^2 for 20 min. Furthermore, non-treated HeLa cells were irradiated with the laser (irradiation control). The experiment was evaluated by MTS assay 24 h after irradiation.

Acknowledgements

This research was funded by CONICYT/MINCyT 2012 Projects (PCCI12-038), FONDECYT1140660, FONDAP ACCDiS15130011, and Funded by Program U-Redes, Vice-presidency of Research and Development, University of Chile. FonCyT, CONICET and SeCyT-UNRC. Cavallo thanks CONICET for fellowships. D. Acevedo and E. Yslas are permanent research fellows of CONICET.

Appendix A. Supplementary data

Supplementary data associated with this article can be found, in the online version, at http://dx.doi.org/10.1016/j.colsurfb.2016.05.060.

References

[1] F.C. Meldrum, Calcium carbonate in biomineralisation and biomimetic chemistry, Int. Mater. Rev. 48 (2003) 187–224.
[2] O. Grassmann, G. Müller, P. Löbmann, Organic-inorganic hybrid structure of calcite crystalline assemblies grown in a gelatin hydrogel matrix: relevance to biomineralization, Chem. Mater. 14 (2002) 4530–4535.
[3] S. Mann, G.A. Ozin, Synthesis of inorganic materials with complex form, Nature 382 (1996) 313–318.
[4] A. Neira-Carrillo, D.F. Acevedo, M.C. Miras, C.A. Barbero, D. Gebauer, H. Cölfen, J. Arias, Influence of conducting polymers based on carboxylated polyaniline on in vitro CaCO3 crystallization, Langmuir 24 (2008) 12496–12507.
[5] H. Cölfen, Precipitation of carbonates: recent progress in controlled production of complex shapes, Curr. Opin. Colloid Interface Sci. 8 (2003) 23–31.
[6] M. Mihai, I. Bunia, F. Doroftei, C.-D. Varganici, B.C. Simionescu, Highly efficient copper(II) ion sorbents obtained by calcium carbonate mineralization on functionalized cross-linked copolymers, Chemistry 21 (2015) 5220–5230.
[7] M.G. Ma, Y.Y. Dong, L.H. Fu, S.M. Li, R.C. Sun, Cellulose/CaCO3 nanocomposites: microwave ionic liquid synthesis, characterization, and biological activity, Carbohydr. Polym. 92 (2013) 1669–1676.
[8] Y. Svenskaya, B. Parakhonskiy, A. Haase, V. Atkin, E. Lukyanets, D. Gorin, R. Antolini, Anticancer drug delivery system based on calcium carbonate particles loaded with a photosensitizer, Biophys. Chem. 182 (2013) 11–15.
[9] N. Qiu, H. Yin, B. Ji, N. Klauke, A. Glidle, Y. Zhang, et al., Calcium carbonate microspheres as carriers for the anticancer drug camptothecin, Mater. Sci. Eng. C 32 (2012) 2634–2640.
[10] J. Wei, T. Cheang, B. Tang, H. Xia, Z. Xing, Z. Chen, Y. Fang, W. Chen, A. Wu, S. Wang, J. Luo, The inhibition of human bladder cancer growth by calcium

carbonate/CaIP6 nanocomposite particles delivering AIB1 siRNA, Biomaterials 34 (2013) 1246–1254.
[11] S. Gopi, V.K. Subramanian, K. Palanisamy, Aragonite-calcite-vaterite: a temperature influenced sequential polymorphic transformation of CaCO3 in the presence of DTPA, Mater. Res. Bull. 48 (2013) 1906–1912.
[12] B. Julia, I. Introduction, C. Sanchez, B. Julián, P. Belleville, M. Popall, Applications of hybrid organic–inorganic nanocomposites, J. Mater. Chem. 15 (2005) 3559–3592.
[13] S. Mridha, D. Basak, ZnO/polyaniline based inorganic/organic hybrid structure: electrical and photoconductivity properties, Appl. Phys. Lett. 92 (2008) 142111–142113.
[14] C.-W. Hsiao, E.-Y. Chuang, H.-L. Chen, D. Wan, C. Korupalli, Z.-X. Liao, et al., Photothermal tumor ablation in mice with repeated therapy sessions using NIR-absorbing micellar hydrogels formed in situ, Biomaterials 56 (2015) 26–35.
[15] F. Zhou, D. Xing, Z. Ou, B. Wu, D.E. Resasco, W.R. Chen, Cancer photothermal therapy in the near-infrared region by using single-walled carbon nanotubes, J. Biomed. Opt. 14 (2009) 21007–21009.
[16] D. Jaque, L.M. Maestro, B. del Rosal, P. Haro-Gonzalez, A. Benayas, J.L. Plaza, E.M. Rodríguez, J. García Solé, Nanoparticles for photothermal therapies, Nanoscale (2014) 1–35.
[17] V. Shanmugam, S. Selvakumar, C.-S. Yeh, Near-infrared light-responsive nanomaterials in cancer therapeutics, Chem. Soc. Rev. (2014) 6254–6287.
[18] Q. Liu, C. Sun, Q. He, D. Liu, A. Khalil, T. Xiang, et al., Ultrathin carbon layer coated MoO2 nanoparticles for high-performance near-infrared photothermal cancer therapy, Chem. Commun. (Camb.) 51 (2015) 10054–10057.
[19] A.R. Guerrero, N. Hassan, C.A. Escobar, F. Albericio, M.J. Kogan, E. Araya, Gold nanoparticles for photothermally controlled drug release, Nanomedicine (Lond.) 9 (2014) 2023–2039.
[20] R. Weissleder, A clearer vision for in vivo imaging, Nat. Biotechnol. 19 (2001) 316–317.
[21] L.E. Ibarra, E.I. Yslas, M.A. Molina, C.R. Rivarola, S. Romanini, C.A. Barbero, et al., Near-infrared mediated tumor destruction by photothermal effect of PANI-Np in vivo, Laser Phys. 23 (2013) 066004–066007.
[22] J. Zhou, Z. Lu, X. Zhu, X. Wang, Y. Liao, Z. Ma, et al., NIR photothermal therapy using polyaniline nanoparticles, Biomaterials 34 (2013) 9584–9592.
[23] D. Gao, L. Gao, C. Zhang, H. Liu, B. Jia, Z. Zhu, F. Wang, Z. Liu, A near-infrared phthalocyanine dye-labeled agent for integrin αvβ6-targeted theranostics of pancreatic cancer, Biomaterials 53 (2015) 229–238.
[24] A. Sahu, W. Il Choi, J.H. Lee, G. Tae, Graphene oxide mediated delivery of methylene blue for combined photodynamic and photothermal therapy, Biomaterials 34 (2013) 6239–6248.
[25] P. Vijayaraghavan, R. Vankayala, C.-S. Chiang, H.-W. Sung, K.C. Hwang, Complete destruction of deep-tissue buried tumors via combination of gene silencing and gold nanoechinus-mediated photodynamic therapy, Biomaterials 62 (2015) 13–23.
[26] L. Li, Y. Liu, P. Hao, Z. Wang, L. Fu, Z. Ma, J. Zhou, PEDOT nanocomposites mediated dual-modal photodynamic and photothermal targeted sterilization in both NIR I and II window, Biomaterials 41 (2015) 132–140.
[27] R. Sierpe, E. Lang, P. Jara, A.R. Guerrero, B. Chornik, M.J. Kogan, N. Yutronic, Gold nanoparticles interacting with β-Cyclodextrin-Phenylethylamine inclusion complex: a ternary system for photothermal drug release, ACS Appl. Mater. Interfaces 7 (2015) 15177–15188.
[28] E.S. Shibu, M. Hamada, N. Murase, V. Biju, Nanomaterials formulations for photothermal and photodynamic therapy of cancer, J. Photochem. Photobiol. C: Photochem. Rev. 15 (2013) 53–72.
[29] P. Cavallo, D.F. Acevedo, M.C. Fuertes, G.J.A.A. Soler-Illia, C. a. Barbero, Understanding the sensing mechanism of polyaniline resistive sensors. Effect of humidity on sensing of organic volatiles, Sens. Actuators B: Chem. 210 (2015) 574–580.
[30] E.I. Yslas, L.E. Ibarra, D.O. Peralta, C.A. Barbero, V.A. Rivarola, M.L. Bertuzzi, Polyaniline nanofibers: acute toxicity and teratogenic effect on Rhinella arenarum embryos, Chemosphere 87 (2012) 1374–1380.
[31] P. Humpolicek, V. Kasparkova, P. Saha, J. Stejskal, Biocompatibility of polyaniline, Synth. Met. 162 (2012) 722–727.
[32] T.A. Skotheim, R.L. Elsenbaumer, J.R. Reynolds, Handbook of Conducting Polymers, Handb Conduct. Polym, CRC Press Taylor & Francis Group, 2007, pp. 847–880.
[33] D.F. Acevedo, M.C. Miras, C.A. Barbero, Solid support for high-throughput screening of conducting polymers, J. Comb. Chem. 7 (2005) 513–516.
[34] E.I. Yslas, P. Cavallo, D.F. Acevedo, C.A. Barbero, V.A. Rivarola, Cysteine modified polyaniline films improve biocompatibility for two cell lines, Mater. Sci. Eng. C 51 (2015) 51–56.
[35] X. Liu, B. Li, F. Fu, K. Xu, R. Zou, Q. Wang, B. Zhang, Z. Chen, J. Hu, Facile synthesis of biocompatible cysteine-coated CuS nanoparticles with high photothermal conversion efficiency for cancer therapy, Dalton Trans. 43 (2014) 11709–11715.
[36] R. Kesarkar, M. Yeole, B. Dalvi, M. Sharon, A. Chowdhary, Simplistic approach towards synthesis of highly stable and biocompatible L-cysteine capped gold nanosphere intermediate for drug conjugation, Int. J. Pharm. Sci. Rev. Res. 31 (2015) 143–146.
[37] L. Mu, Y. Gao, X. Hu, L-Cysteine: a biocompatible, breathable and beneficial coating for graphene oxide, Biomaterials 52 (2015) 301–311.
[38] D.A. Acevedo, A.F. Lasagni, C.A. Barbero, F. Mücklich, Simple fabrication method of conductive polymeric arrays by using direct laser interference micro-/nanopatterning, Adv. Mater. 19 (2007) 1272–1275.
[39] N.S. Sariciftci, H. Kuzmany, H. Neugebauer, A. Neckel, Structural and electronic transitions in polyaniline: a Fourier transform infrared spectroscopic study, J. Chem. Phys. 92 (1990) 4530–4539.
[40] J. Tang, X. Jing, B. Wang, F. Wang, Infrared spectra of soluble polyaniline, Synth. Met. 24 (1988) 231–238.
[41] S. Aryal, B.K.C. Remant, N. Dharmaraj, N. Bhattarai, C.H. Kim, H.Y. Kim, Spectroscopic identification of SAu interaction in cysteine capped gold nanoparticles, Spectrochim. Acta A: Mol. Biomol. Spectrosc. 63 (2006) 160–163.
[42] M. Grzeszczuk, A. Grańska, R. Szostak, Raman spectroelectrochemistry of polyaniline synthesized using different electrolytic Regimes-Multivariate analysis, Int. J. Electrochem. Sci. 8 (2013) 8951–8965.
[43] M. Jain, S. Annapoorni, Raman study of polyaniline nanofibers prepared by interfacial polymerization, Synth. Met. 160 (2010) 1727–1732.
[44] G. Behrens, L.T. Kuhn, R. Ubic, A.H. Heuer, Raman spectra of vateritic calcium carbonate, Spectrosc. Lett. 28 (1995) 983–995.
[45] H. Cölfen, M. Antonietti, Crystal design of calcium carbonate microparticles using double-hydrophilic block copolymers, Langmuir 14 (1998) 582–589.
[46] R. Vacassy, J. Lemaître, H. Hofmann, J.H. Gerlings, Calcium carbonate precipitation using new segmented flow tubular reactor, AIChE J. 46 (2000) 1241–1252.
[47] H.J. Salavagione, D.F. Acevedo, D.E. Grumelli, F. Garay, G.A. Planes, G.M. Morales, Novel synthetic methods to produce functionalized conducting polymers I. Polyanilines, Electrochim. Acta. 49 (2004) 3671–3686.
[48] P. Villalba, M.K. Ram, H. Gomez, V. Bhethanabotla, M.N. Helms, A. Kumar, A. Kumar, Cellular and in vitro toxicity of nanodiamond-polyaniline composites in mammalian and bacterial cell, Mater. Sci. Eng. C 32 (2012) 594–598.
[49] Z. Kucekova, P. Humpolicek, V. Kasparkova, T. Perecko, M. Lehocký, I. Hauerlandová, et al., Colloidal polyaniline dispersions: antibacterial activity, cytotoxicity and neutrophil oxidative burst, Colloids Surf. B: Biointerfaces 116 (2014) 411–417.
[50] S. Schmidt, D. Volodkin, Microparticulate biomolecules by mild CaCO3 templating, J. Mater. Chem. B 1 (2013) 1210–1218.
[51] G.B. Sukhorukov, D. Volodkin, A.M. Gunther, A.I. Petrov, D.B. Shenoy, H. Mohwald, Porous calcium carbonate microparticles as templates for encapsulation of bioactive compounds, J. Mater. Chem. 14 (2004) 2073–2081.
[52] X. Ma, L. Li, L. Yang, C. Su, Y. Guo, K. Jiang, Preparation of highly ordered hierarchical CaCO3 hemisphere and the application as pH value-sensitive anticancer drug carrier, Mater. Lett. 65 (2011) 3176–3179.
[53] D. Volodkin, CaCO3 templated micro-beads and −capsules for bioapplications, Adv. Colloid Interface Sci. 207 (2014) 306–324.
[54] Y. Zhang, P. Ma, Y. Wang, J. Du, Q. Zhou, Z. Zhu, X. Yang, J. Yuan, Biocompatibility of porous spherical calcium carbonate microparticles on hela cells, World J. Nano Sci. Eng. 02 (2012) 25–31.
[55] D.V. Volodkin, N.I. Larionova, G.B. Sukhorukov, Protein encapsulation via porous CaCO3 microparticles templating, Biomacromolecules 5 (2004) 1962–1972.
[56] C. Peng, Q. Zhao, C. Gao, Sustained delivery of doxorubicin by porous CaCO3 and chitosan/alginate multilayers-coated CaCO3 microparticles, Colloids Surf. A: Physicochem. Eng. Asp. 353 (2010) 132–139.
[57] D. Zhao, C.J. Liu, R.X. Zhuo, S.X. Cheng, Alginate/CaCO3 hybrid nanoparticles for efficient codelivery of antitumor gene and drug, Mol. Pharm. 9 (2012) 2887–2893.
[58] S.A. Kamba, M. Ismail, S.H. Hussein-Al-Ali, T.A.T. Ibrahim, Z.A.B. Zakari, In vitro delivery and controlled release of Doxorubicin for targeting osteosarcoma bone cancer, Molecules 18 (2013) 10580–10598.
[59] M. Ayad, G. El-Hefnawy, S. Zaghlol, Facile synthesis of polyaniline nanoparticles; its adsorption behavior, Chem. Eng. J. 217 (2013) 460–465.
[60] C. Zapata-Urzua, M. Perez-Ortiz, G.A. Acosta, J. Mendoza, L. Yedra, S. Estrade, A. Álvarez-Lueje, L.J. Núñez-Vergara, F. Albericio, M.J. Lavilla, M.J. Kogan, Hantzsch dihydropyridines: privileged structures for the formation of well-defined gold nanostars, J. Colloid Interface Sci. 453 (2015) 260–269.